PERGAMON

International Journal of Heat and Mass Transfer 41 (1998) 3469–3482

International Journal of HEAT and MASS TRANSFER

Prediction of thermal contact resistance between polished surfaces

E. G. Wolff*, D. A. Schneider†

Department of Mechanical Engineering, Oregon State University, Corvallis, OR 97331, U.S.A.

Received 26 September 1997; in final form 27 January 1998

Abstract

Various theories have been formulated to predict thermal contact resistance but agreement with experiments has been variable when very smooth surfaces are involved. The guarded hot plate method for thermal conductivity measurements was chosen to determine temperature drops across interfaces. It was shown that a general theory can be modified to give a good estimation of the thermal resistance with a variety of interface materials. The effects of pressure, material hardness, surface roughness, and thermal properties of the interface material on thermal resistance between two smooth steel surfaces were studied. Air, Cu, In and Teflon foils, a silicone oil based heat sink compound and Ag filled paint were studied. The theory predicts temperature discontinuities when solids, fluids or gases are present in the interface.

Nomenclature

A surface or interface area [m^2]
a accommodation coefficient
B gap number
b intercept for heat flow at zero time
C constriction number
C_p specific heat at constant pressure
E emissivity of the contact surfaces evaluated at T_1 or T_2
h interface conductance [W/K] $= 1/R = q/\Delta T$
K conductivity number
k thermal conductivity [W/m-K]
k_o gas conductivity at zero contact pressure
k_1, k_2 conductivities of the two solids evaluated at T_1 and T_2
M Meyer hardness [kg mm^{-2} or same units as p] of softer material
MW molecular weight
m temperature correction
N effective gap coefficient (EGC)
P load in kg
p contact pressure [kg mm^{-2} or same units as M]
Pr Prandtl number
Q heat flux [W m^{-2}] $= q/A$
q heat [W]
R contact resistance [K/W]
S interface size number
T temperature [K]
t interface foil thickness [m]
U conductance number
u contact conductance/area [W m^{-2} K^{-1}] $= h/A$, also thermal contact conductance [TCC]
V free volume
v' mean molecular velocity [cm s^{-1}].

Greek
γ ratio of specific heats
δ effective distance between surfaces [m]
δ_i surface roughness mean depth [m]
μ dynamic viscosity [g/cm-s]
v the kinematic viscosity [μ/ρ] evaluated at t_i [cm^2 s]
ρ density [g cm^{-3}] of gas or fluid at interface
σ the Stefan–Boltzmann radiation constant [5.670 e^{-8} W/(m^2*K^4)].

Subscripts
ac actual
av average

* Corresponding author.
† Present address: Precision Measurements and Instruments Corporation, Philomath, OR 97370, U.S.A.

0017–9310/98 $19.00
PII: S0017–9310(98)00067–2

c actual contact spot
o fluid, zero contact pressure
m arithmetic mean
1, 2 solid #, surface #
f equivalent fluid
s solid.

1. Introduction

Thermal contact conductance or resistance is of interest in many fields including internal combustion engineering, bearings with lubrication, heat transfer across granular solids [1], microelectronics [2], superconductors [3], aerospace structures [4, 5], and biomedical prosthetics [6]. Whenever heat flow or energy transfer at the interface of two materials must be estimated or controlled, or the temperature drop across the interface known, then contact conductance data/predictions must be available. Thermal conductance data are also required in the measurement of the thermal conductivity (k) of a solid. In the guarded hot plate method [7, 8] a one dimensional heat flow is set up along the length of a 'stack,' which consists of a heat source, heat sink, the material under question and a heat flow sensor. Given the temperature gradient and heat flow, Fourier's first law can be used to calculate the conductivity. A frequent objective of thermal conductivity measurements is also to find materials which minimize thermal resistances. The same data help to minimize losses at any connections to cold or heat sources.

2. Background

Heat flow between two solids in contact was not widely studied before 1943, when Alcock [1] pointed out that surfaces could be modeled as the touching of multiple peaks or asperities. The basic one-dimensional model consists of parallel heat flow through the asperities and the interfacial material. The conductance depends on contact pressure, the thermal conductivity, hardness, surface finish, and both the size and shape of the contacting irregularities. The trend to lumped parameters and their ratios was begun. Convection and radiation heat transfer represent a negligible energy transfer [5, 9].

Limited work on measurement and theory in the late 1940s and 1950s was summarized by Fenech and Rohsenow [10] who extended the model of contact at discrete points to a method for calculating the thermal conductance of any combination of metals, surface states and fluid in the voids at the temperature and pressure desired. Considerable work in this field was carried out in the 1960s. Veziroglu (having as a student [11] worked with M. Fishenden [12] on the subject), finally summarized the general theory and correlated the data from numerous results (e.g. [4]) based on stainless steel and aluminum contact surfaces, contact pressures of 0.0035–0.3 kg mm^{-2}, RMS surface roughness of 0.25 to 3 μm and air, brass shim stock or asbestos sheets as an interface material. As such, the theory [13] has been established in the handbooks [14].

Since then, various related theories have been formulated to predict thermal conductance for a variety of conditions. Agreement with experiments has been variable [3–6, 9, 15–17], especially when very smooth surfaces are involved. In order to correlate the analytical and measured contact conductance it is first necessary to measure and quantify the finish of the opposing surfaces. These may range from machined, ground, sanded and bead blasted to highly polished. In general, the bead blasted surface results more closely matched the analytical models than did the sanded or ground surfaces [15]. This is because of the homogeneous distribution of asperities on the bead blasted surface. The ground and sanded surfaces have a directionally dependent roughness causing long wave-length undulations which makes it much more difficult to predict the actual contact ratio (the true contact area of the asperity tips divided by the nominal area). It has been found that applied pressure affects the contact conductance to varying degrees. For nominally very smooth surfaces, and for hard materials, the applied pressure has little effect [14]. For rougher surfaces, and if one or both of the surfaces is composed of a material that can deform easily at either the microscopic or macroscopic level, then the pressure can affect the contact conductance. While discrepancies are often due to lack of precise input parameters, we shall show that a general theory can be modified to give a good estimation of the thermal resistance with a variety of interface materials.

3. Theory

The general theoretical model for thermal conductance is based on Veziroglu [13, 14]. An effective gap thickness is described by:

$$\delta = N\{\delta_1 + \delta_2\} \tag{1}$$

where N equals the slope of a 'best' fit line through the empirical data points of the sum of surface roughness versus the effective gap thickness. Veziroglu determined $N = 3.56$ for $(\delta_1+\delta_2) < 7.0$ μm and 0.46 if > 7 μm. The effective fluid thermal conductivity is determined by:

$$k_f = k_o \tag{2}$$

if the interstitial fluid is a liquid and

$$k_f = \frac{k_o}{1 + \dfrac{8\gamma(v/v')(a_1 + a_2 - a_1 a_2)}{100\delta\, Pr\, a_1 a_2(\gamma+1)}} + \frac{4\sigma\delta E_1 E_2 T_m^3}{E_1 + E_2 - E_1 E_2} \tag{3}$$

if it is a gas. The factor of 100 is for consistent units.

The conductivity number K is found from:

$$K = k_f\left[\frac{k_1+k_2}{2k_1k_2}\right] \tag{4}$$

where the individual conductivities are calculated at the actual contact spots and at the mean temperature of the respective surface temperatures, defined as:

$$T_c = \frac{k_1T_1+k_2T_2}{k_1+k_2}. \tag{5}$$

The constriction number C is defined as:

$$C = \sqrt{p/M} \tag{6}$$

while the interface size number S is:

$$S = \sqrt{A}/\delta. \tag{7}$$

The gap number, B, is the relationship between the constriction number and the interface size number:

$$B = 0.335C^{0.315S^{0.137}}. \tag{8}$$

The exponential coefficients were derived by fitting a line to the correlation data. The conductance number can be found by iteration of the following transcendental equation:

$$U = 1+\frac{BC}{K\tan^{-1}\{(1/C)(1-(1-U))^{0.5}-1\}} \tag{9}$$

or graphically from Fig. 1 using C and B/K [13]. The conductance is then:

$$u(\mathrm{TCC}) = h/A = Uk_f/\delta. \tag{10}$$

The predicted temperature drop will be:

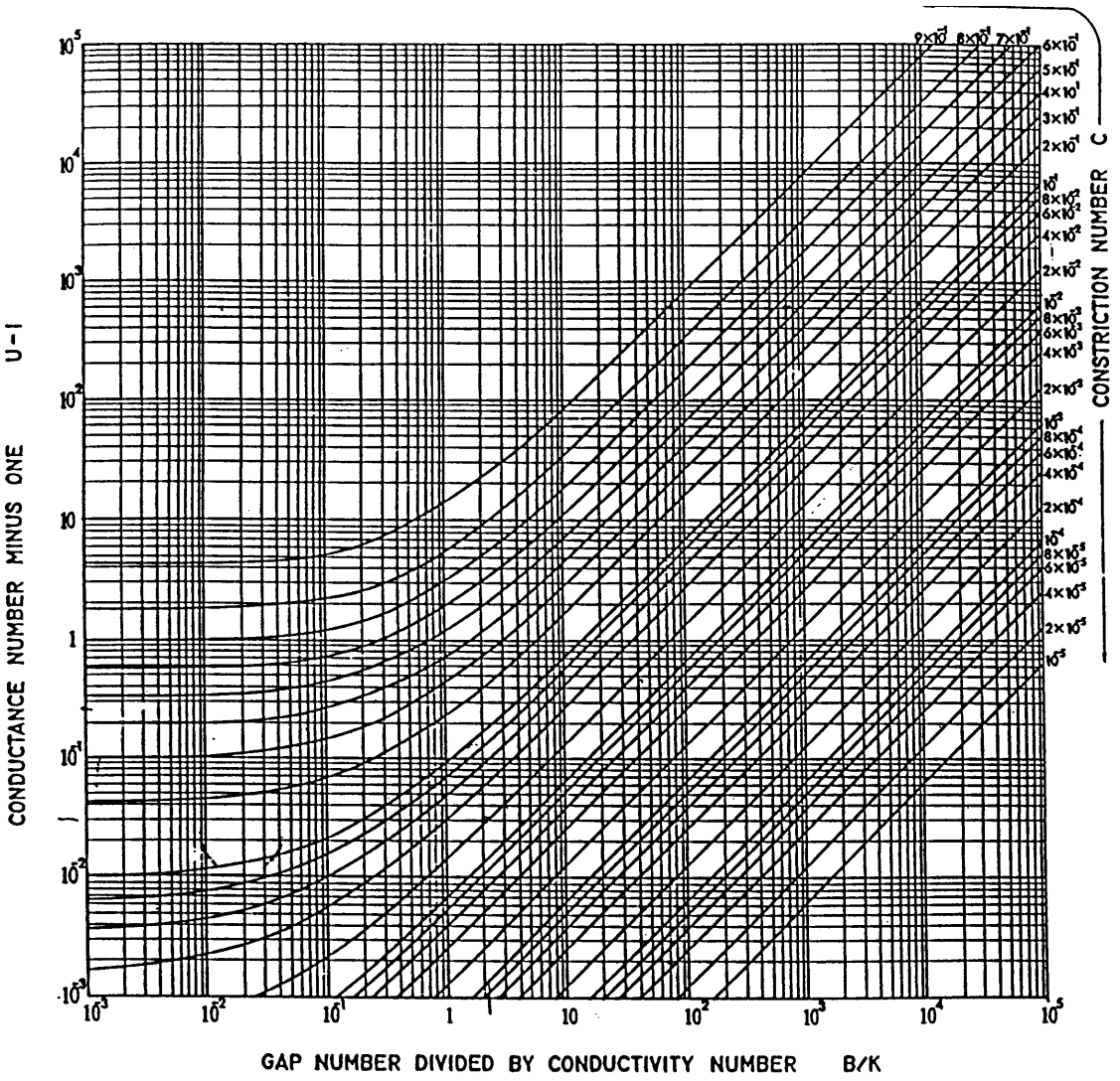

Fig. 1. Chart for calculating thermal contrast conductance [13].

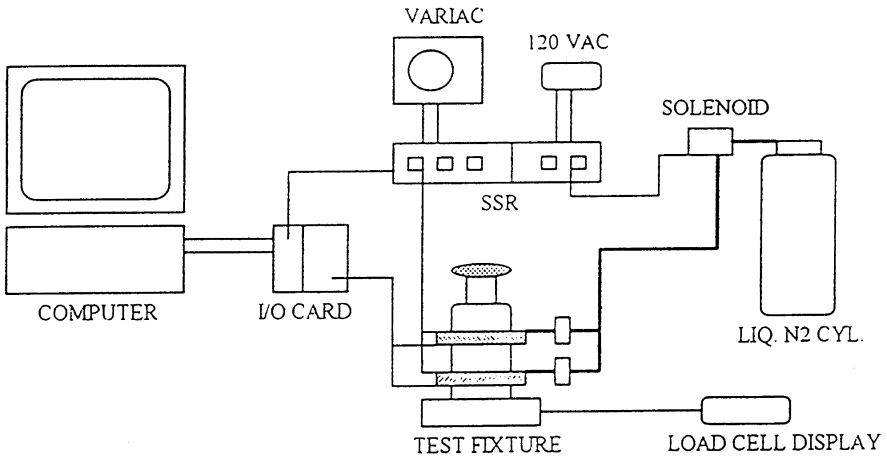

Fig. 2. Test apparatus.

$$\Delta T = Q/u = (\delta * Q)/(U * k_f). \quad (11)$$

Note that B, C, S, K and U are all dimensionless numbers, so the units of p must only match M, and the contact area must be the square of the units used for δ.

4. Experimental

4.1. Apparatus

In order to obtain accurate data for modeling, the experimental approach (Fig. 2) was to establish a heat source and a heat sink to maintain a steady state heat flow along the longitudinal axis of a test specimen. The temperature gradient and heat flux along this axis were measured to obtain either the sample conductivity or interface conductances. The apparatus [18] included a guarded hot plate fixture, solid state relays, solenoid valve, liquid nitrogen tank, load cell with digital display and an AC variac. The radial heat losses were minimized to help account for all heat transfer. The compression force exerted in the longitudinal direction of the test piece was measured. The guarded hot plate fixture (Fig. 3) was constructed of copper upper and lower plates, stainless

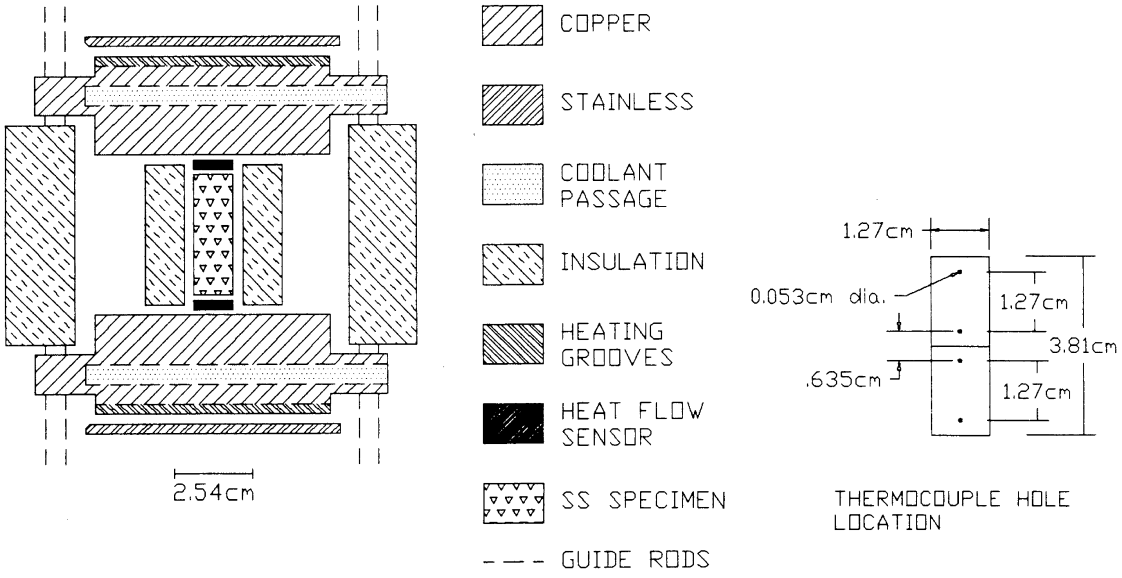

Fig. 3. Guarded hot plate with insulation and test specimen.

steel guide rods and plates, and aluminum support pieces. The large knurled knob at the top of the fixture controlled the clamping load while a load cell at the bottom monitored the load applied uniformly via a ball bearing under the bottom plate and a rounded tip on the clamping rod. Centrally located thermocouples provided the signal for temperature monitoring by the analog input part of the data acquisition system. Digital output from the card operated the solid state relays which cycled on and off to control current to the resistance heating and liquid nitrogen solenoid.

The copper upper and lower plates (Fig. 3) provided the temperature differential to drive the energy transfer. The plates contained passageways for liquid nitrogen cooling and grooves for resistance heating. The coolant passages were drilled into the solid copper in a double-J pattern, with the unnecessary holes and passages tapped and plugged. The inlet and exhaust ports were fitted with barb type fittings for connection with rubber hoses. The heating grooves were machined into the surface of the plates opposite the contact surface. Nichrome wires contained in ceramic ferrules were put in the grooves and held in position with stainless steel plates, chosen for their relatively low thermal conductivity and high heat tolerance. Radial heat losses were minimized by a passive guard heater. A glass-ceramic (Zerodur) disc was placed between the stack and the load cell for thermal isolation (Fig. 2).

The steel contact surfaces were finished on 600 grit wet/dry sandpaper, with a unidirectional sanding motion. This produced a surface roughness of 0.0708 μm (RMS) parallel to the sanding marks and 0.0482 μm (RMS) perpendicular to the sanding marks as measured with a Tencor Instruments Alpha-Step 100. All the test pieces were machined from the same bar stock and in the same direction, to eliminate possible inconsistency due to material anisotropy such as texture.

4.2. Procedures

All tests were performed at between 0 and 100°C in 20° steps in air with either 20, 30 (standard) or 40°C (ΔT) temperature differences across the stack. The sample temperature profile, the temperatures of the upper and lower plates and the heat flow were recorded at 30 s intervals. For each successive test the interface material was changed and/or the pressure was changed. Table 1 lists the details of various interface materials and pressures tested. Typically, the final ten data points at each temperature step were averaged for calculation of the desired information. Given the temperature gradient between the thermocouples and the distance to the interface, the temperature at each side of the interface was found by extrapolation. The difference between adjacent surface temperatures was then the drop across the interface. The contact resistance was found by dividing this number by the heat flux as measured by the heat flow sensors.

Heat flow information during testing was provided by a pair of thermopile based heat flow sensors (Concept Engineering FS-60) with same area as test specimens. One each was placed at the top and bottom of the stack, nearest to the hot and cold plates. The output from the sensors was voltage, calibrated to W m^{-2}. The sensors were additionally checked with a standard stainless steel, thermal conductivity reference material NIST-SRM-1462. The SRM had 0.024 inch diameter holes drilled from the side at a carefully measured distance apart, in which 0.003 inch diameter wire T-type thermocouples were inserted. Because the conductivity of the SRM as a function of temperature was known, the temperature

Table 1
Test details

Test #	ΔT (°C)	Material	Interface thickness (μm)	Tests loads (kg)	Comments
#1–3	30	None	0	0, 22.7, 90.7	Steel blocks only
#4–8	30	Indium foil	38	11.3, 22.7, 45.3, 113, 22.7	Same foil
#9, 10	30	99.99%		113.4, 113.4	New foil
#11–14	30	Teflon tape Mil-Spec T-27730A	25.4	11.3, 22.7, 45.3, 113.4	New foil/test
#15–17	30	Heat sink compound		11.3, 22.7, 113.4	New film/test
#18–21	30	Silver paint		11.3, 22.7, 45.3, 113.4	New coating/test
#22–25	30	Copper foil	38	11.3, 22.7, 45.4, 113.4	Same foil
#26	30	(Annealed)		113.4	New foil
#27	20	Heat sink compound		22.7	New film
#28	40		25.4	22.7	Same film as #27
#29	20	Teflon tape		45.3	New film
#30	40			45.3	Same film as #29

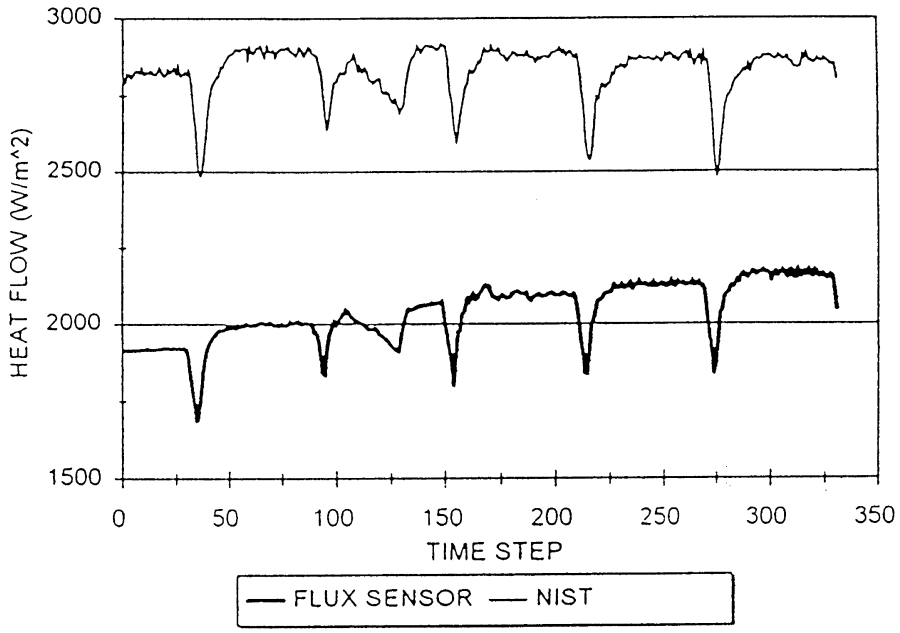

Fig. 4. Sensor calibration data for 30°C temperature drop across fixture.

gradient between the thermocouples could then be used to calculate the true heat flow using Fourier's equation for one-dimensional heat flow. (Assuming a worst case emissivity of 0.9 [17], the radiant heat transfer correction was only 10.36 W m^{-2} or 0.38% maximum error at 100°C.)

It was found that the true heat flow number derived from the gradient in the SRM was approximately 50% higher than the value indicated by the heat flow sensors, and was also dependent on the average temperature at which the measurement was taken. Figure 4 shows the raw data obtained from a typical calibration test. The lower line is the average of the heat flux sensor outputs, while the upper line is the computed heat flux based on the temperature gradient in the NIST SRM. The periodic dip in each curve corresponds to the transition from one temperature step to the next. This is caused by the lag in temperature rise in the test specimen due to its heat capacity. As the test fixture ramped up to the next higher temperature step, the upper heat flow sensor recorded a higher flux. But because the lower plate was temporarily hotter than the test specimen there was a reversal of heat flow through the lower flux sensor. The average of the output from the two heat sensors then showed a lower value until the test specimen approached the desired average temperature. The reason for the extra dip in each curve between the 100th and 150th time step is not certain, but may have something to do with an imbalance in the liquid nitrogen flow.

Inspection of Fig. 4 indicates that the true steady state heat flow is relatively constant with time (and temperature), while the average output of the heat flux sensors (Q_{av}) is approximately a linear function of temperature. A straight line superimposed over either curve would coincide with the steady state portion of the data. Due to the apparent linearity of both curves, correction for true heat flux used the relation:

$$Q_{ac}/Q_{av} = mT + b. \tag{12}$$

A linear regression was performed on the data shown in Fig. 4, (with a correlation coefficient of 0.99942) and this procedure allowed superposition of the two curves and correction for the true heat flux, and also at all test temperatures.

The first test was performed on a steel sample with no gap, as baseline for all subsequent tests. Figure 5 shows that the temperature profile of the solid specimen, at an average temperature of 100°C is consistent with Fourier's first law. The effectiveness of the passive guard heater was verified because the heat flux is constant along the length of the piece. If the radial heat losses were significant, or the sample had not yet reached steady state, this would result in a curved temperature profile.

5. Results

Table 2 lists the surface temperatures, interface temperature differences and the thermal contact conductances (TCC) for average sample temperatures of 0°C

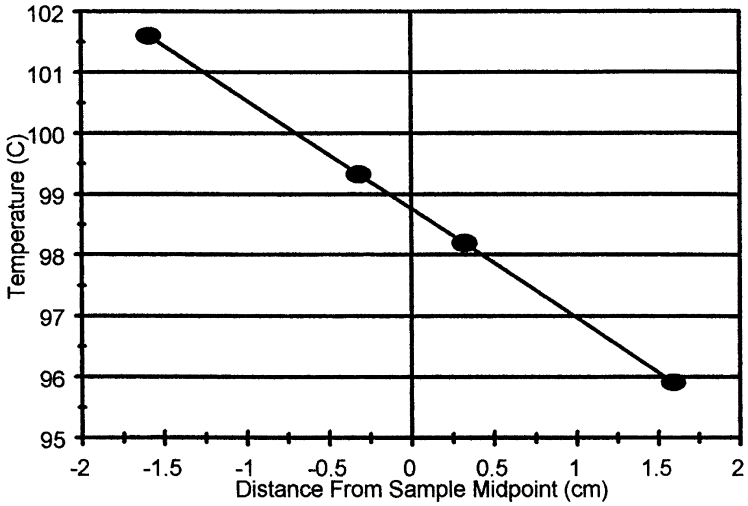

Fig. 5. Temperature profile of solid specimen at $T_m = 100°C$ (no interface).

Table 2
Experimental results for average sample temperatures of 0°C and 100°C with a 30°C fixture temperature difference

		Data at 0°C				Data at 100°C			
Interface material	Load (kg)	T_h (°C)	$T1$ (°C)	ΔT (°C)	TCC (W m^{-2} K^{-1})	T_h (°C)	$T1$ (°C)	ΔT (°C)	TCC (W m^{-2} K^{-1})
None	22.7	−0.85	−1.85	1	2696	98.88	97.89	0.994	2727
	90.7	−0.58	−1.61	1.03	2607	99.11	98.2	0.916	3007
Indium foil	11.3*	−0.57	−1.64	1.07	2533	99.04	98.1	0.943	2891
	22.7**	−0.88	−1.9	1.02	2659	99.06	98.21	0.852	3205
	45.3**	−0.58	−1.6	1.02	2643	99.1	98.21	0.894	3080
	113.4**	−0.64	−1.49	0.85	3174	99.03	98.23	0.793	3489
Teflon tape	11.3*	0.16	−2.01	2.18	1176	99.03	97.65	1.381	1901
	22.7*	−0.49	−2.20	1.71	1532	99.05	97.82	1.231	2188
	45.3*	−0.61	−1.07	0.46	5799	98.95	98.48	0.464	5886
	113.4*	−0.66	−1.03	0.37	7489	98.75	98.33	0.415	6617
Heat sink compound	11.3*	−0.77	−0.86	0.14	19837	98.38	98.14	0.248	11026
	22.7*	−0.57	−0.83	0.27	10253	98.59	98.37	0.221	12574
	113.4*	−0.66	−0.84	0.18	15683	98.49	98.35	0.141	19717
Silver paint	11.3*	−0.79	−1.04	0.25	11014	98.46	98.19	0.271	10213
	22.7*	−1.19	−1.45	0.26	10618	98.51	98.49	0.021	130845
	45.3*	−0.96	−1.28	0.32	8771	98.43	98.26	0.175	15765
	113.4*	−0.78	−0.95	0.17	16352	98.44	98.23	0.205	13645
Copper foil	11.3*	−0.48	−2.18	1.7	1572	98.92	97.58	1.341	1975
	22.7**	−0.39	−2.00	1.63	1628	98.88	97.62	1.262	2131
	45.3**	0.01	−1.46	1.47	1835	98.84	97.71	1.131	2393
	113.4**	0.06	−1.25	1.31	2102	98.76	97.77	0.994	2736
	113.4*	−0.08	−1.21	1.12	2649	98.99	98.13	0.88	3197

* New interface material.
** Interface material from previous test.

and 100°C with a 30°C temperature drop across the stainless steel sample ($Q = 2700$ W m^{-2}). The results follow the trend of increasing conductance with increasing temperature and pressure. The Teflon tape, indium foil and copper foil show the most increase in conductance with increasing pressure, while the heat sink compound and silver paint show less of this tendency. Most of the samples show some increase in conductance with increasing temperature, although this trend is not consistent in all of the samples.

5.1. Air gap

A split sample with no interface material was tested at 22.68 kg and 90.72 kg loads. The sample temperature profiles for both tests are shown in Fig. 6. While the temperature range differs somewhat between the two loads, the gradients are similar and interface temperature drops differ by less than 8%. As would be expected, the test with the higher load had the smaller temperature drop across the interface. Another important feature of this graph is the comparison between profiles for the solid piece, in Fig. 5, and split test piece in Fig. 6. While the two profiles for the split test piece are nearly parallel, they have a shallower slope than the solid test piece. This is caused by the added resistance of the interface, which is not present in the solid piece, resulting in a slight decrease in heat flow and gradient. The slope of the temperature profile ($\delta T/\delta x$) is also constant on either side of the interface for each of the tests. Table 2 indicates that the interface temperature drop remains constant at about 1°C. These pressures are probably too low to cause deformation and the resultant increased contact area for a material as hard as stainless steel.

5.2. Annealed copper foil

This material was first cleaned with 600 grit wet/dry sandpaper, heated in a propane torch for annealing and treated with a flux containing zinc chloride and hydrochloric acid, followed by a water rinse. There was a distinct trend towards lower contact resistance with increasing pressure. In a second identical test with new foil at a 113.4 kg load, the temperature drop was less at each data point than for the previous 113.4 kg test. This may be attributed to a softer new copper foil which deformed more readily, compared to work hardening of the prior foil from the loading cycles.

5.3. Indium foil

This is a soft metal with a conductivity of 24 W m^{-1} K^{-1}. The data (Table 2) show a slight decrease in temperature drop (increase in conductance) with increasing pressure. Repeat tests on the same foil suggest that there is not only a pressure dependence, but that the conductance might also be a function of deformation due to time, temperature and maybe even the number of loading and temperature cycles. However, inspection and measurement of the indium foil after testing showed no permanent thinning (to $\pm 0.0005''$).

5.4. Teflon tape

In this series of tests, the interface temperature drops decreased through the 11.3, 22.7 and 45.3 kg tests, but level off for the 113.4 kg test. Inspection of the Teflon tape after each test showed substantial and uneven thinning. It appears that at the 45.3 kg load the flow stress of the

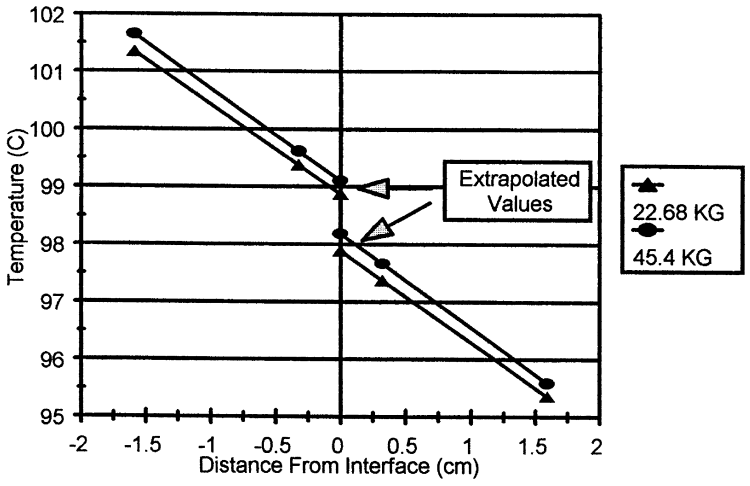

Fig. 6. Temperature profile of split test piece with no interface material.

material has been exceeded, giving no benefit to increased loading. The conductance may also be aided by Teflon's lubricating ability [8]. The uneven thinning may be evidence of non-flat (wavy) contact surfaces, or non-parallel contact. At 45.3 and 113.4 kg load, the temperature drop (0.5°C) is less than that for no interface material and indium foil (1.0°C).

The same Teflon tape was retested at the 45.3 kg load with varying heat flux levels so that the temperature drop across the sample was 20°C and also 40°C. The interface temperature drop was generally proportional to the fixture ΔT as predicted by eqn 11. In other words, the temperature drop with a 40°C ΔT was about twice the temperature drop with a 20°C ΔT, especially at the higher mean temperatures. The conductance showed an unusual trend in that at the lower end of the test range the two values are different.

5.5. *Heat sink compound* (*HSC*)

This material, composed of 70% polysiloxane (silicone oil) and 30% zinc oxide, is commercially available from Radio Shack/Tandy Corporation as Product #276-1372. The temperature drop was constant (0.2°C) over the pressure range. Even at 11.3 kg the flow stress of the material was exceeded. In spite of a low conductivity (0.4 W m^{-1} K^{-1}), the wetting ability of the oil improves the contact conductance. As theorized earlier, it is probably the low flow stress more than the conductivity of the interface material that improves the conductance [3, 8]. At the conclusion of each test, the oil was cleaned from the contact surfaces and replaced. At this time it was observed that the oil was thicker and more viscous than at the beginning of the test. Apparently the testing had changed the properties, perhaps by boiling off some of the more volatile materials.

The heat sink compound was also tested with different heat fluxes (temperature drops of 20°C and 40°C). At a loading of 22.6 kg there was a slight variation of conductance with mean temperature at a gradient of 20°C. The test with a 40°C differential showed very nearly the same temperature drop as the original test, but had a consistently higher conductance. As this test used the same interface material as the previous test, it is possible the silicone oil underwent a property change during the first test, possibly due to the more volatile components boiling off. The conductance was not a constant but its (derived) value was very sensitive to a change in the temperature drop.

5.6. *Silver paint*

This material, supplied by Energy Beam Sciences, (#P-CS-30) was used undiluted. Besides silver and proprietary resins, it contains ethyl cellosolve, isopropyl alcohol, MEK, ethyl acetate and xylene. It was removed after each test, using the solvent/extender supplied with the paint. As Table 2 indicates, there is no apparent pressure effect on the conductance or temperature drop. The drop was 0.2–0.3°C over the temperature range, and there is no apparent trend due to pressure.

6. Mathematical model

The results of Table 2 for an air interface ($\Delta T = 1.0$°C at 0°C) are initially compared to predictions from Veziroglu's model for conductance [13]. Predictions and parameters for eqns (1)–(13) are summarized in Table 3. The constant N is initially taken as = 3.56 (for $\delta_1+\delta_2 < 7.0$ μm) [7, 13]. Using eqns (1)–(8) we find $C = 0.0243$ and $B/K = 2.47$. Using Fig. 1 we find $U = 1.05$ and eqn (11) predicts $\Delta T = 0.0767$ K. The most likely cause of the discrepancy between this predicted and the measured value of 1.0°C is considered to be the expression for the effective gap thickness, eqn (1). The reason for this is that the predicted temperature is based on eqn (11), where Q is measured and all parameters needed for the factors U, and k_f are well known. Figure 7, taken from Veziroglu [13], shows the data for 0.2 μm $<(\delta_1+\delta_2) < 7$ μm on which $N = 3.56$ was based. Additional data are summarized in [13] for $\delta_1+\delta_2$ up to 90 μm. There is considerable scatter in all data. Our measured surface roughness of the stainless steel test pieces was $\delta_1+\delta_2 = 0.1188$ μm, which is significantly smoother than the data used to formulate the correlations. Inspection of Fig. 7 shows that there is a distinct group of data points at the low end of the surface roughness scale, which has a nearly vertical alignment. A line drawn through this subset of points (regression analysis not requiring the curve to go through zero) would have a slope substantially greater than the 3.56 predicted for the set as a whole. It is believed that this distinct trend for relatively smooth contact surfaces is caused by the macro-roughness, or waviness of the surface. As the surfaces get smoother, the waviness supersedes the micro-roughness as the dominant factor controlling the effective gap thickness.

Figure 8 compares the data of [13] for the three size ranges 0.2–0.7 μm, 0.7–7 μm and 7–90 μm by regression analyses with and without constraining the curves to go through zero. Since our data for the air gap suggests an EGC or N value of about 84 (at $\delta_1+\delta_2 = 0.1158$ μm), the results of Fig. 8 indicate this value is consistent with the trends of Fig. 7 and total data of [13].

The value of $N = 84$ and/or the curve of Fig. 8, is used to predict the results of all further experiments (with the same steel blocks). For interface materials other than a gas, two additional steps are required. Interface foils such as In, Teflon and copper act by creating two interfaces, viz. two steel–foil interfaces. In this case the total ΔT is given by:

Table 3
Thermal conductance predictions

Parameter	Units	Data source	Air	Copper		Teflon		Indium	HSC	Ag paint
Surface 1	—	NIST	Steel	Steel		Steel		Steel	Steel	Steel
Fluid	—	—	Air	Air		Air		Air	HSC	Ag paint
Foil	—	—	None	Cu	Cu	Teflon	Teflon	In	None	None
t	m	measure	N/A	0.0000381		0.0000254		0.0000381	N/A	N/A
Surface 2	—	—	Steel	Cu	Cu	Teflon	Teflon	In	Steel	Steel
Temperature	K	measure	0°C	0	0	0	0	0	0	0
Q	W m^{-2} K^{-1}	measure	2700	2700	2700	2700	2700	2700	2700	2700
load	kg	measure	22.7	22.7	113.4	22.7	113.4	22.7	22.7	22.7
M	kg mm^{-2}	measure	190	(100)	190	(2)	(2)	(25)	190	190
P	kg mm^{-2}	measure	0.1125	0.1125	0.5625	0.1125	0.5625	0.1125	0.1125	0.1125
A	m^2	measure	0.0002016	0.0002016		0.0002016		0.0002016	0.0002016	0.0002016
δ_1	m	measure	7.080 e^{-08}	7.080 e^{-08}		7.080 e^{-08}		7.080 e^{-08}	7.080 e^{-08}	7.080 e^{-08}
δ_2	m	measure	4.800 e^{-08}	(1 e^{-7})	4.080 e^{-08}	4.800 e^{-08}		(6 e^{-8})	4.800 e^{-08}	4.800 e^{-08}
N (EGC)	—	Eqn (13)	84	59	84	84		−76	84	84
C (int)	cal g K^{-1}	[22]	0.2404	0.2404		0.2404		0.2404	0.42	0.1
C_p (suf)	cal g K^{-1}	[22]	0.106	0.106		0.106		0.106	0.106	0.106
a_1, a_2	—	[23]	0.9	0.9		0.9		0.9	(1)	(1)
Pr	—	[14]	0.7	0.7		0.7		0.7	(1)	(1)
μ	g cm s^{-1}	[14]	0.000175	0.000175		0.000175		0.000175	1	3500
ρ (fluid)	g/cc	[22]	0.001293	0.001293		0.001293		0.001923	2.3	6.4
v'	cm s	[22]	44700	44700		44700		44700	720	600
k_1	W m^{-1} K^{-1}	[24]	13.775	13.775		13.775		13.775	13.775	13.775
k_2	W m^{-1} K^{-1}	[22]	13.775	384		0.28		24	13.775	13.775
k_o	W m^{-1} K^{-1}	[22]	0.024	0.024		0.024		0.024	0.42	350
C	—	Eqn (6)	0.0243	0.0335	0.054	0.237	0.53	0.067	0.024	0.024
B/K	—	Eqns (4) and (8)	8.35	24.1	31.2	2.3	4.59	25.2	2.17	1.98
U	—	Fig. 1	1.15	1.45	2	1.55	6	2.2	1.05	1.03
ΔT	K	Eqn (11)	0.99	0.8	0.541	0.746	0.19	0.523	0.285	0.265
ΔT (cond)	K	Eqn (13)	N/A	0.00027	0.00027	0.0245	0.0011	0.0043	N/A	N/A
ΔT (pred)	K	Eqn (13)	0.99	1.6	1.08	1.74	0.386	1.05	0.29	0.265
ΔT (meas)	K	Table 1	1	1.63	1.12	1.71	0.37	1.02	0.27	0.26

Estimated values are in parentheses; references are in brackets.

Table 4
Uncertainty calculations for selected experiments [14]

Parameters			Uncertainty		
Interface material	Load (kg)	T (°C)	Interface temperature drop (%)	Heat flux (%)	Contact conductance (%)
None	22.7	0	11.45	5.49	12.7
None	22.7	100	11.0	5.49	12.3
Heat sink compound	113.4	0	67.53	5.48	67.75
Heat sink compound	113.4	100	80.7	5.48	80.9
Teflon tape	11.3	0	5.18	5.49	7.55
Teflon tape	11.3	100	7.62	5.48	9.39
Teflon tape	113.4	0	33.47	5.49	33.91
Teflon tape	113.4	100	27.93	5.49	28.47

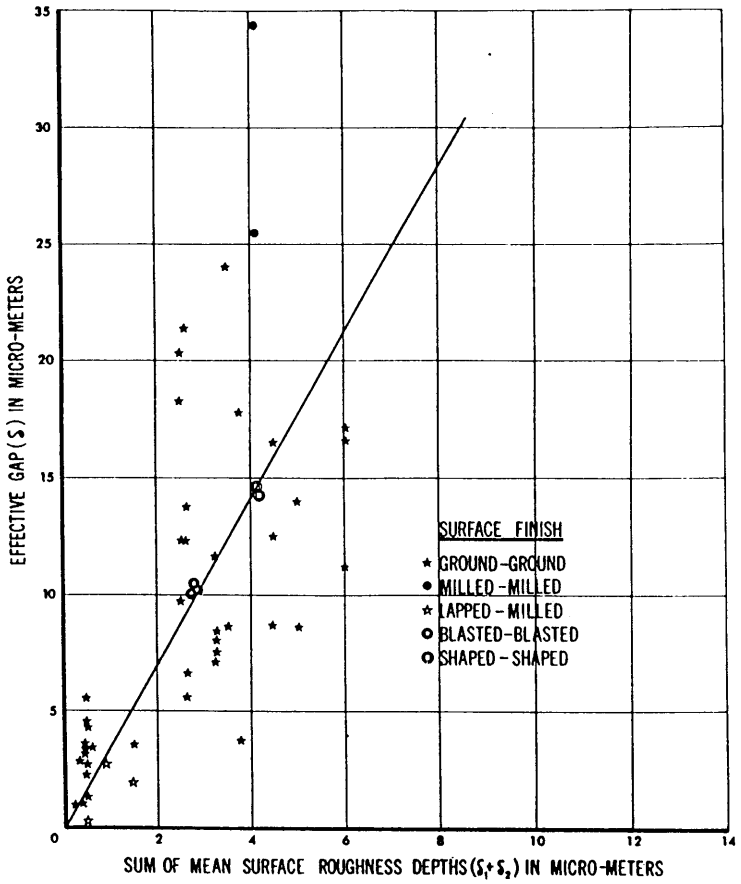

Fig. 7. Effective gap vs sum of surface roughness mean depths for smooth contacts ($\delta_1+\delta_2 < 7$ μm) [13].

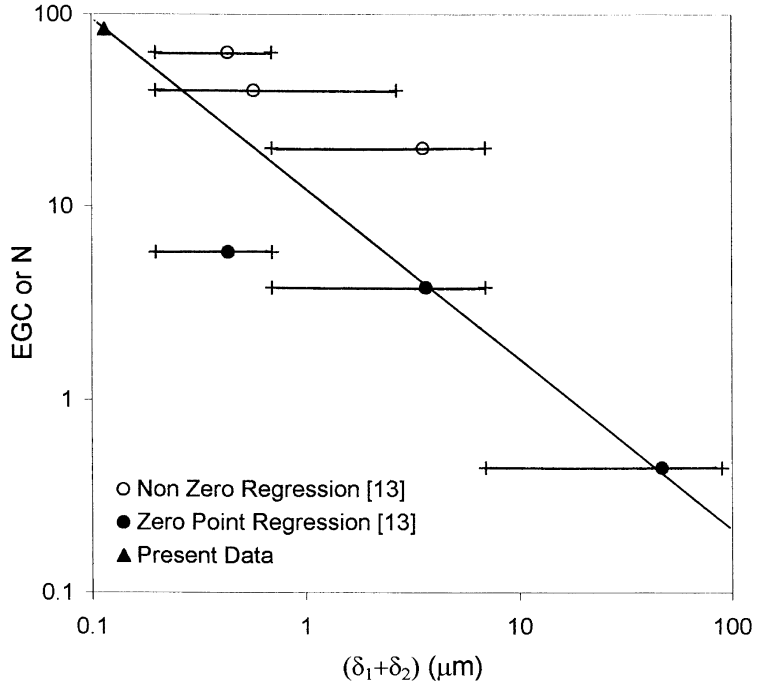

Fig. 8. Data of Fig. 7 and Veziroglu [13] for EGC vs $(\delta_1+\delta_2)$ compared for zero and non-zero reference slopes.

$$\Delta T = \Delta T(\text{steel–foil}) + \Delta T(\text{foil–steel}) + Qt/k. \tag{13}$$

The foil–steel interfaces are treated as above, having an air interface and using the M value to correspond to the softer material. The last term is a thermal resistance due merely to the thickness of the foil. This may be generalized to

$$\Delta T = Q(\Sigma u^{-1} + \Sigma t_i/k_i) \tag{14}$$

where the summation is over the total number of interfaces and slabs involved.

The predictions in Table 3 for Cu, In and Teflon foil interfaces are straightforward and require only measured or well estimated values of the Meyer hardness. The latter is based on the projected area of an indentation rather than the surface area used in Brinell hardness testing and is less sensitive to applied load. While we have used the similar and more accessible Brinell hardness measurement (with the same units), the Meyer test should be considered [19]. The surface roughness of the foils here are estimated; it is assumed that the lower the hardness the closer the surface roughness will correspond to the (measured) roughness of the harder (steel) material, especially with an increase in pressure.

The values for air are well known and one can qualitatively assume that μ and Pr increase while v' decreases for the denser compounds. Predictions for the heavy or filled fluids, the heat sink compound and the silver paint, are more difficult. The original theory claims that for a fluid $k_f = k_o$ [eqn (2)]. This does not work for the interface materials (too low a ΔT is predicted) and an increase in the second term of the denominator of eqn (3) is called for. The major unknown materials' lumped parameter is:

$$\frac{v}{Pr * v'} = \frac{\mu}{\rho}\frac{k_o}{C_p * \mu}\frac{1}{v'} = \frac{k_o}{C_p * \rho}\frac{1}{v'}. \tag{15}$$

The present data suggest this lumped parameter is 6 e^{-4} for the HSC and 0.91 for the Ag paint. Since k_o, C_p and ρ can be estimated for the compounds (see Table 3), we can derive the effective mean molecular velocities v'. We obtain $v' = 720$ cm s^{-1} for the HSC (silicone oil based), with v/Pr about 0.43 cm^2 s^{-1}. The corresponding figures for the Ag paint are 600 cm s^{-1} for v' and 547 cm^2 s^{-1}.

In a grease or liquid polymer, discrete molecular collisions do not occur and heat is transferred by phonon collisions whose velocity depends on Umklapp processes, the phonon mean free path. Nevertheless, viscosity tends to increase with molecular weight (e.g., [20]), which implies a decrease in molecular mobility. Viscous forces between molecules can also be related to the sharing of velocities between molecules in a liquid [21]. The relation suggested was

$$v' \backsimeq \mu V_f^{2/3} M\mathrm{W}^{-1} \tag{16}$$

where V_f is the free volume. Data on μ and MW of the respective liquid compounds are currently unavailable.

7. Conclusions

Materials used to reduce thermal contact resistance were tested at the interface of stainless steel blocks with the aid of a thermal conductivity test fixture. Clamping loads ranged from 11.3–113.4 kg, and average temperatures ranged from 0°C–100°C. Interface materials included silicone based heat sink compound, Teflon tape, silver filled paint, indium foil and annealed copper foil.

The ability of the interface material to conform to the surface of the opposing materials appears to be a greater factor than the conductivity of the material. It was found that a silicone based heat sink compound and a silver filled paint improved the conductance more than did metallic foils such indium or annealed copper. The ability of the heat sink compound and the silver paint to conduct energy at the interface was independent of the applied load. The Teflon tape showed increasing conductance with increasing load up to 45.4 kg, but little improvement when the load was increased to 113.4 kg. Both the indium foil and annealed copper foil showed an increase in conductance as the load was increased, with no indication that a limit had been reached within this load range. The conductance of most of the materials tested appeared to increase slightly with increasing test temperature. This trend is most apparent in the copper and indium foils and the Teflon tape at lower pressures. There also appears to be some interdependence with the flow stress of the material. The silicone grease and silver paint showed no dependence on either the test temperature or the pressure. The Teflon tape conductance showed a dependence on temperature at lower pressures, but none above the loading at which the flow stress had apparently been exceeded. The metallic foil conductances increased with temperature at all pressure loading. Data suggest that if the flow stress of the foils had been reached the conductance would have been unaffected by the test temperature. With the heat sink compound, Teflon tape and silver paint it appeared that increasing the pressure would have no further effect on the conductance. But with the harder materials, i.e. indium foil and copper foil, the trend to increased conductance with increasing pressure had not reached a maximum. Data for the harder materials indicate that the conductance continued to change with the test temperature, even up to the maximum temperature, perhaps because of the temperature dependency of the conductivity and flow stress.

The original mathematical model [13] failed to accurately predict the effective gap thickness for very smooth contact surfaces. Extrapolation of regression analyses suggests the data of Veziroglu [13] support the apparent trend to higher gap coefficients. When interface foils were employed, the theory was successfully extended by considering the total interface as two solid/foil interfaces in air plus the conductance through the solid foil. Heavy fluid interface materials such as heat sink compounds and paints can be handled theoretically by assuming an equivalent gas medium with appropriate adjustment of $\mu/Pr * v'$. Ideally these should be based on knowledge of the free volume and molecular weights of the fluids, but for practical purposes, the derived values from this work can guide predictions for related materials.

Acknowledgements

The authors wish to thank members of the staff of Precision Measurements and Instruments Corporation (PMIC), especially Matthew Norris and Richard J. Oram, for valuable suggestions.

References

[1] Alcock JF. Communications on a review of recent progress in heat transfer. Proceedings Institution of Mechanical Engineers 1943;149:126.
[2] Lambert MA, Fletcher LS. Metallic coatings for enhancement of thermal contact conductance. Journal of Thermophysics and Heat Transfer 1994;8:341–8.
[3] Ochterbeck JM, Peterson GP, Fletcher LS. Thermal contact conductance of metallic coated BiCaSrCuO superconductor/copper interfaces at cryogenic temperatures. ASME/JSME Thermal Engineering Proceedings 1991;1:275–84.
[4] Barzelay ME, Tong KN, Holloway GF. Effect of pressure on thermal conductance of contact joints. Technical Note 3295, National Advisory Committee for Aeronautics, Washington, 1955.
[5] Giommi M, Torrisi FR, Marchetti M, Testa P. Measurement of thermal conductivity and thermal contact resistance in composite materials for space applications. Sixth International Conference on Composite Materials (ICCM-VI). Elsevier, London, 1987, Paper 4.323.
[6] Parmenter KE, Maddren J, Marschall E. Thermal contact resistance of dissimilar pressed metal contacts in a vacuum environment. Thermal Conductivity Conference #22, 1994.
[7] ASTM C-177-85. Standard Test Method for Steady-State Heat Flux Measurements and Thermal Transmission Properties by Means of the Guarded-Hot-Plate Apparatus. American Society of Testing and Materials, 1991.
[8] ASTM C-518-91. Standard Test Method for Steady-State Heat Flux Measurements and Thermal Transmission Properties by Means of the Heat Flow Meter Apparatus. American Society of Testing and Materials, 1991.
[9] Hsieh CK, Touloukian YS. Correlation and prediction of thermal contact conductance for nominally flat surfaces. 8th Conference on Thermal Conductivity, Plenum Press, 1968.
[10] Fenech H, Rohsenow WM. Prediction of thermal con-

duction of metallic surfaces in contact. Journal of Heat Transfer, Trans ASME, 1963;85:15–24.
[11] Cetinkale TN. Minutes of proceedings of meetings held in March 1945. Proceedings of Institution of Mechanical Engineers, 1945;152:141.
[12] Centinkale TN, Fishenden M. Thermal conductance of metal surfaces in contact. International Conference on Heat Transfer. Institution of Mechanical Engineers (London), 1951.
[13] Veziroglu TN. Correlation of thermal contact conductance experimental results. Progress in Astronautics and Aeronautics 1967;20:Academic Press, New York.
[14] Rohsenow WM, Hartnett JP. Handbook of Heat Transfer. McGraw-Hill, New York, 1973.
[15] McWaid T, Marschall E. Thermal contact resistance across pressed metal contacts in a vacuum environment. International Journal of Heat Mass Transfer 1992;35:2911–20.
[16] Currie TC, Rogers JT. Heat transfer between rough surfaces in contact over a highly elliptical contour area : comparison of experimental and numerical results. Proceedings of the Eighth International Heat Transfer Conference 1986; pp. 639–44.
[17] Blanchard DG, Fletcher LS. Contact conductance of selected metal-matrix composites. Journal of Thermophysics and Heat Transfer 1995;9:391–4.
[18] Schneider D. Thermal contact resistances in a thermal conductivity test system. M.Sc. Thesis, Oregon State University, Department of Mechanical Engineering, 1998.
[19] Dieter GE. Mechanical Metallurgy. McGraw-Hill Book Co., 1986; 327.
[20] Tollefson NM, Roy S, Shepard TA. Effects of additives on molecular weight correlations to dynamic viscosity on polypropylenes. Polymer Engineering and Science 1996;36:117–25.
[21] Suryanarayana CV. Propagation of ultrasonic waves in liquids : a new model. Ultrasonics 1992;30:104–6.
[22] Handbook of Chemistry and Physics, 42nd edn. The Chemical Rubber Publishing Co., Ohio, 1960.
[23] Eid JC, Antonetti VW. Small scale thermal contact resistance of aluminum against silicon. Proceedings of 8th International Heat Transfer Conference 1986; 659–63.
[24] National Bureau of Standards, SRM 1462, Austenitic Stainless Steel.